A fine-tuned vector-parasite dialogue in tsetse's cardia determines peritrophic matrix integrity and trypanosome transmission success

Aurélien Vigneron[1*], Emre Aksoy[1,#a], Brian L Weiss[1], Xiaoli Bing[1,#b], Xin Zhao[1,#c], Erick O Awuoche[1,#d], Michelle O'Neill[1], Yineng Wu[1], Geoffrey M Attardo[1,#e], Serap Aksoy[1]

[1] Department of Epidemiology of Microbial Diseases, Yale School of Public Health, New Haven, Connecticut, United States of America

[#a]Current Address: Graduate Program in Genetics, Genomics and Bioinformatics, University of California Riverside, Riverside, California, United States of America

[#b]Current Address: Department of Entomology, Cornell University, Ithaca, New York, United States of America

[#c]Current Address: CAS Key Laboratory of Pathogenic Microbiology and Immunology, Institute of Microbiology, Chinese Academy of Sciences, Beijing, China

[#d]Current Address: Department of Agriculture, School of Agriculture and Food Science, Meru University of Science and Technology, Meru, Kenya

[#e]Current Address: Department of Entomology and Nematology, University of California Davis, Davis, California, United States of America

*Corresponding author
E-mail: aurelien.vigneron@yale.edu (AV)

Keywords: tsetse; trypanosome; peritrophic matrix; reactive oxygen species; vector-parasite interaction

Abstract

Arthropod vectors have multiple physical and immunological barriers that impede the development and transmission of parasites to new vertebrate hosts. These include the peritrophic matrix (PM), a chitinious barrier that separates the blood bolus from the midgut epithelia and modulates the vector-microbiota interactions. In tsetse flies, a sleeve-like PM is continuously produced by the cardia organ located at the fore- and midgut junction. During their development in tsetse, African trypanosomes have to bypass the PM twice: first to colonize the midgut and then to reach the salivary glands (SG). However, not all flies with midgut infections develop mammalian transmissible SG infections - the reasons for which are unclear. Here, we used transcriptomics, microscopy and functional genomics analyses to dissect the factors that regulate parasite migration from midgut to SG. In flies with midgut infections only, parasites are cleared at the cardia by reactive oxygen intermediates (ROIs) at the expense of collateral cytotoxic damage to the cardia. In flies with midgut and SG infections, gene expression for components of the PM is reduced and structural integrity of the barrier is compromised. Under these circumstances trypanosomes traverse through the layers of the PM by aggregating into cyst-like bodies. The process of PM attrition that enables the parasites to reenter into the midgut lumen to move forward to SG is apparently mediated by components of the parasites residing in the cardia. Thus, a fine-tuned dialogue between tsetse and trypanosomes at the cardia determines the outcome of PM integrity and trypanosome transmission success.

Author summary

Insects are responsible for transmission of parasites that cause deadly diseases in humans and animals. Understanding the key factors that enhance or interfere with parasite transmission processes can result in new control strategies. Here, we report that a proportion of tsetse flies with African trypanosome infections in their gut can prevent the parasites from migrating to the salivary glands, albeit at the expense of collateral damage. In a subset of flies with gut infections, the parasites manipulate the integrity of the gut barrier, called the peritrophic matrix, and reach the salivary glands for transmission to the next mammal. Either targeting parasite manipulative processes or enhancing peritrophic matrix integrity could reduce parasite transmission.

Introduction

Insects are essential vectors for the transmission of microbes that cause devastating diseases in humans and livestock. Many of these diseases lack effective vaccines and drugs for control in the mammalian hosts. Hence, reduction of insect populations, as well as approaches that reduce the transmission efficiency of pathogens in insect vectors, are explored for disease control. Tsetse flies transmit African trypanosomes, which are the causative agents of human and animal African trypanosomiases. These diseases can be fatal if left untreated and inflict significant socio-economic hardship across a wide swath of sub-Saharan Africa [1, 2]. The phenomenon of antigenic variation the parasite displays in its mammalian host has prevented the development of vaccines, and easily administered and affordable drugs are unavailable. However, tsetse population reduction can significantly curb disease, especially during times of endemicity [3, 4]. In addition, strategies that reduce parasite transmission efficiency by the tsetse vector can prevent disease emergence. A more complete understanding of parasite-vector dynamics is essential for the development of such control methods.

For transmission to new vertebrate hosts, vector-borne parasites have to first successfully colonize their respective vectors. This requires that parasites circumvent several physical and immune barriers as they progress through their development in the vector. One prominent barrier they face in the midgut is the peritrophic matrix (PM), which is a chitinous, proteinaceous membrane that separates the epithelia from the blood meal [5-7]. In *Anopheles* mosquito the presence of the PM benefits the vector by regulating the commensal gut microbiota and preventing the microbes from invading the hemocoel [8]. In tsetse and sand flies, the PM plays a crucial role as an infection barrier by blocking parasite development and colonization [9, 10]. The presence of the PM can also be exploited by microbes to promote their survival in the gut lumen. The agents of Lyme disease, *Borrelia burgdorferi*, bind to the tick vector gut and exploit the PM for protection from the harmful effects of blood-filled gut lumen [11]. Unlike the adult female mosquito gut that produces a type I PM in reponse to blood feeding, tsetse's sleeve-like type II PM is constitutively produced by the cardia organ, which is located at the junction of the fore- and midgut. Upon entering the gut lumen, long-slender bloodstream (BSF) trypanosomes are lysed while short-slender BSFs differentiate to midgut-adapted procyclic forms (PCF) [12]. During these lysis and differentiation processes, BSF parasites shed their dense coat of variant surface glycoproteins (VSGs) into the midgut environment [12]. These molecules are internalized

by cells in the cardia, where they transiently inhibit the production of a structurally robust PM. This process promotes infection establishment by enabling trypanosomes to traverse the PM barrier and invade the midgut ectoperitrophic space (ES) [9]. After entering the ES, trypanosomes face strong epithelial immune responses, which hinder parasite gut colonization success. Detection of PCF parasites in the ectoperitrophic space induces the production of trypanocidal antimicrobial peptides [13, 14], reactive oxygen intermediates (ROIs) [15], PGRP-LB [16] and tsetse-EP protein [17]. These immune effectors eliminate trypanosomes from the majority of flies. In the end, only in a small percentage of flies PCF parasites remain in the midgut and move to the cardia. They next differentiate into long and short epimastigote forms and have to reenter the gut lumen to migrate through the foregut into the salivary glands (SG), where they differentiate to mammalian infective metacyclic forms [18, 19]. However, only a percentage of flies that have midgut infections will go on to develop SG infections that are necessary for disease transmission. The physiological mechanisms that prevent midgut parasites from infecting the SG remain unknown.

In this study, we investigated the molecular and cellular mechanisms that enable the parasites to escape from the ectoperitrophic space of the midgut for successful SG colonization. Our results show that tsetse can restrict parasite survival in the cardia via induction of oxidative stress, although this resistance is costly and results in extensive damage to cellular physiology. In contrast, tolerance to parasite transmission represents a more homeostatic state and requires that the parasites successfully bypass the PM barrier in the cardia. We discuss the molecular interactions that regulate this complex and dynamic vector-parasite relationship in the cardia, an essential organ for disease transmission.

Results and Discussion

Trypanosome infection dynamics in tsetse

Tsetse display resistance to infection with trypanosomes. Following ingestion, parasites successfully colonize the midgut and cardia of only a small percentage of flies. Furthermore, not all gut infections give rise to mature metacyclics in the SG, in which case transmission to a subsequent vertebrate host fails (Fig 1A). Hence, two forms of fly infections exist: non-permissive infections when parasites are restricted exclusively to the gut (hereafter designated 'inf+/-'), and permissive infections where parasites are present in the gut and SGs (hereafter designated 'inf+/+') (Fig 1B). Why only some of the midgut-infected tsetse individuals support trypanosome colonization of the SGs remains unknown. To begin addressing this question, we investigated whether parasites from non-permissive (inf+/-) gut infections suffer a bottleneck that results in the selection of cells that lack the ability to progress in development to metacyclic infections in the SG. We challenged two groups of teneral adults (newly eclosed) *per os* with *Trypanosoma brucei brucei* parasites obtained from midguts of either inf+/+ or inf+/- flies. We observed a similar proportion of inf+/+ and inf+/- phenotypes regardless of the initial parasite population (inf+/+ or inf+/-) used for challenge (Fig 1C). This result indicates that trypanosomes in the inf+/- gut population are developmentally competent, and can give rise to SG metacyclics. Thus, we reasoned that the cardia physiological environment may determine the developmental course of trypanosome infection dynamics.

Parasites bypass the PM and enter into the gut lumen in permissive (inf+/+) cardia

To investigate the molecular aspects of the crucial bottleneck that limits parasite transmission in the inf+/- group, we fed mammalian BSF parasites (*Trypanosoma brucei brucei* RUMP 503) to teneral adults and 40 days later dissected and pooled infected cardia into inf+/- and inf+/+ groups (*n*=3 biological replicates per group, with 10 cardia per replicate). For comparison, we similarly obtained dissected cardia from age-matched normal controls (called non-inf; *n*=3 biological replicates per group, with 10 cardia per replicate). We next applied high-throughput RNA-sequencing (RNA-seq) to profile the gene expression in the three groups of cardia. We obtained on average > 23M reads for each of the 9 libraries, with 77.8% (non-inf), 75.4% (inf+/-) and 64.5% (inf+/+) of the total reads mapping to *Glossina morsitans morsitans* transcriptome (S1 Fig). The trypanosome reads corresponded to about 3.5% in non-permissive (inf+/-) dataset and

about 11.9% in the permissive (inf+/+) dataset (Fig 2A). We measured relative parasite density in inf+/- and inf+/+ cardia by quantitative real time PCR (qRT-PCR) using the trypanosome housekeeping gene *gapdh* normalized to tsetse *gapdh*. We found significantly higher parasite density in inf+/+ cardia compared to inf+/- cardia (Student t-test, $p = 0.0028$; Fig 2B). We confirmed that inf+/+ cardia had higher parasite density by counting trypanosome numbers in the cardia using a hemocytometer (S2 Fig). Thus, the difference in the representative parasite transcriptome reads in the two infected groups of cardia is due to an increase in the number of trypanosomes in the inf+/+ cardia rather than an increase in parasite transcriptional activity. Interestingly, we noted no difference in the number of trypanosomes present in inf+/- and inf+/+ midguts (S2 Fig). Hence, it appears that the decrease in parasite density occurs in the cardia despite the fact that similar densities are maintained in the midgut.

Tsetse's cardia is composed of several different cell-types with potentially varying functions (schematically shown in Fig 2C; S3 Fig) [20-22]. These include cells originating from the foregut, which are enclosed within a glandular structure formed by secretory cells originating from the midgut. The organ is surrounded by muscles that form a sphincter around the foregut, which likely regulates blood flow during the feeding process. Additionally, large lipid-containing cells are localized under a layer of muscle below the sphincter, the function of which remains unclear. Microscopy analysis of infected cardia supported our previous molecular findings as we observed fewer parasites in the cardia of inf+/- (Fig 2D) compared to inf+/+ flies (Fig 2E). Parasites from inf+/- cardia were restricted to the ES, whereas inf+/+ cardia had parasites in both the ES and in the lumen. Hence, the parasite populations resident in inf+/+ cardia had translocated from ES to the lumen, while parasites in inf+/- cardia failed to bypass the PM barrier. These data suggest that the cardia physiological environment may influence the parasite infection phenotype and transmission potential.

PM is compromised in permissive (inf+/+) cardia but not in non-permissive (inf+/-) cardia

For succesful transmission, trypanosomes that reside in the ES of the midgut must traverse the PM barrier a second time in order to reenter into the gut lumen, move forward through the foregut and mouthparts and colonize the SGs. This process is thought to occur in the cardia [6, 19] because newly synthesized PM in this niche likely provides a less robust barrier. We investigated whether the functional integrity of the PM in the two different infection states varied in the cardia

organ. We mined the non-inf cardia transcriptome dataset (S1 Dataset) and identified 14 transcripts associated with PM structure and function [6, 9, 23], which cumulatively accounted for 35.7% of the total number of reads based on CPM value (Fig 3A). The same set of genes represented 26.5% and 34.5% of the inf+/+ and inf+/- transcriptome data sets, respectively (Fig 3A). Thus, PM-associated transcripts are less abundant in the inf+/+ cardia relative to inf+/- and control cardia. We next evaluated the expression profile of the PM-associated transcripts and identified those that are differentially expressed (DE) with a fold-change of ≥1.5 in at least one infection state compared to the control (non-inf) (Fig 3B). We observed a significant reduction in cardia-specific transcripts for the major PM-associated Peritrophins (*pro2, pro3)* in the cardia inf+/+, but not the cardia inf+/- dataset. Peritrophins are structural glycoproteins that bind to chitin fibers that make up the PM and influence the elasticity and porosity of the barrier [21]. Interestingly, the expression of *chitinase* was induced in both inf+/- and inf+/+ datasets. Because Chitinase activity can degrade the chitin backbone of the PM, increased levels of its expression would enhance the ability of the parasites to bypass this barrier. Overall, the inf+/+ cardia expression profile we observed here is similar to the profile noted in the cardia 72 hours post BSF parasite acquisition early in the infection process [9]. Results from that study demonstrated that reduced expression of genes that encode prominent PM associated proteins compromised PM integrity, thus increasing the midgut parasite infection prevalence [9]. Loss of PM integrity in the inf+/+ state could similarly enhance the ability of parasites to traverse the PM to re-enter the gut lumen and invade the SGs.

Reduction of PM integrity increases the prevalence of SG infections (inf+/+)

We hypothesized that PM integrity is a prominent factor in the ability of trypanosomes to traverse the barrier in the cardia and continue their migration to the SGs. We addressed this hypothesis by experimentally disrupting the structural integrity of the PM in flies that harbored established gut parasite infections. We modified a dsRNA feeding procedure that targets tsetse *chitin synthase* (dsRNA-*cs*), which has been shown to effectively inhibit the production of a structurally robust PM [7]. We challenged flies with BSF trypanosomes as teneral adults and administered on day 6, 8 and 10 post parasite acquisition blood meals containing dsRNA-*cs*. This is the time interval when we expect the parasites colonizing the ectoperitrophic space of the midgut to bypass the PM barrier in the cardia [19, 24, 25]. Control groups similarly received dsRNA targeting green

fluorescent protein (dsRNA-*gfp*). The decreased expression of *chitin synthase* in the experimental dsRNA-*cs* group relative to the control dsRNA-*gfp* group was confirmed (S4 Fig). Twenty days post dsRNA treatment, midguts and SGs were microscopically dissected and the SG infection status scored. We detected SG infections in 68% of dsRNA-*cs* treatment group compared to 47% in dsRNA-*gfp* control group (Fig 3C). Thus, the PM compromised group of flies showed a significant increase in inf+/+ phenotype relative to the control group (GLM, Wald-test, p=0.0154). These findings suggest that disruption of the PM later in the infection process increases the proportion of gut infected flies that give rise to mature SG infections (inf+/+). Thus, tsetse's PM acts as a barrier for parasite translocation from the ES to the lumen of the midgut, an essential step for successful SG colonization.

Permissive (inf+/+) cardia extracts compromise PM integrity

We sought to determine if components of inf+/+ parasites infecting the cardia could manipulate cardia physiology to bypass the PM using a modified version of a survival assay that was successfully used to evaluate PM structural integrity [7, 9, 26]. In this assay, tsetse with an intact PM fail to immunologically detect the presence of the entomopathogenic *Serratia marcescens* in the gut lumen. The bacteria thus proliferate uncontrolled in this environment, translocate into the hemocoel and kill the fly [7]. Conversely, when PM structure is compromised, the fly's immune system can detect the presence of *Serratia* early during the infection process and express robust antimicrobial immunity that limits pathogen replication and increases host survival [7]. We provided mature adults blood meals supplemented with both entomopathogenic *Serratia* and inf+/+ cardia extracts, while two age-matched control groups received either both *Serratia* and cardia extracts prepared from flies that had cleared their midgut infections (designated rec-/- for "recovered") or only *Serratia* (control). We found that survival of flies that received inf+/+ extracts was significantly higher than either of the two control groups (Fig 3D). These findings suggest that cardia inf+/+ extracts contain molecule(s) that negatively influence tsetse‘s PM integrity, thereby enabling these flies to more rapidly detect *Serratia* and express heightened immune responses to overcome this pathogen.

Our transcriptional investigation indicated that inf+/+ parasites compromise PM associated gene expression while inf+/- parasites did not (Fig 3B). We also found that the density of the parasites colonizing the inf+/- cardia was significantly less than that found in the inf+/+

cardia (Fig 2). We applied the same survival assay using inf+/- cardia extracts containing an equivalent quantity of parasites as that tested in the cardia inf+/+ described above. We observed decreased fly survival when supplemented with the cardia+/- extracts, similar to the two control groups we had used before (Fig 3D). Collectively, these findings confirm that the parasites in cardia inf+/- differ in their ability to interfere with the PM integrity when compared with those in the cardia inf+/+ state. This suggests that parasites in inf+/+ cardia display a different molecular dialogue with tsetse vector tissues.

To understand the cardia-trypanosome interactions, we investigated the parasite populations in the inf+/+ state by EM analysis. We observed that trypanosomes accumulate in the region between the foregut and the midgut parts of the cardia where PM is synthesized (Fig 3E; S5 Fig). Our EM observations also showed that parasites aggregate in compact masses in-between the layers of the PM (Fig 3E; S5 Fig), similar to previously reported "cyst-like" bodies [24]. At the site of some of these aggregates, the luminal layer of the PM appeared disrupted, likely enabling the parasites to escape the barrier. The aggregations we detected in cardia inf+/+ could represent a social behavior that influences cardia-trypanosome interactions and thus parasite transmission success. *In vitro* studies have observed one social behavior, called SoMo for social motility [27], where early-stage PCF parasites (similar to the forms that colonize the fly midgut) cluster and migrate together on semi-agar plates [28]. In the tsetse vector, phases where trypanosomes group in clusters and move in synchrony have been observed during the infection process independent of the developmental stage of the parasite [25]. In addition, these experiments also co-localize parasites in the cardia near the cells that produce the PM, similar to our EM observations.

The cardia from non-permissive infections (inf+/-) is dysfunctional at the cellular level

To obtain a global snapshot of cardia functions that could influence parasite infection outcomes, the DE cardia transcripts between control (non-inf) and either cardia inf+/- or cardia inf+/+ datasets were subjected to Gene Ontology (GO) analysis (using Blast2GO) (S2 Dataset). We noted 88 GO terms that were preferentially down-regulated in the inf+/- state, while only 15 GO terms were down-regulated in the inf+/+ state. The 88 GO terms detected in the inf+/- dataset included 5, 11 and 67 terms associated with mitochondria, muscles and energy metabolism, respectively.

To understand the physiological implications of the inf+/- infection phenotype in the cardia, we investigated the transcriptional responses of the organ as well as the ultrastructural integrity of its mitochondria and muscle tissue. Gene expression patterns indicate that mitochondrial functions are significantly down-regulated in the inf+/- cardia relative to the inf+/+ state (Fig 4A). More specifically, these genes encode proteins associated with energy metabolism, including the cytochrome c complex, the NADH-ubiquinone oxidoreductase and the ATP-synthase that function at the organelle's inner membrane. Loss of mitochondrial integrity was further demonstrated by microscopic analysis of cardia muscle cells (Fig 4B-D) and fat-containing cells (Fig 4E-G). In the cardia inf+/- phenotype, EM observations showed mitochondrial degradation around myofibrils associated with muscle cells (Fig 4C), while few such patterns were noted in the control cardia (Fig 4B) and cardia inf+/+ (Fig 4D). The mitochondria within the lipid containing cells of both inf+/- and inf+/+ presented a disruption in the cristae organization, suggesting a disruption of the inner membrane (Fig 4F-G), in support of transcriptomic level findings (Fig 4A).

In addition to putative mitochondrial proteins, we found that the expression of genes encoding structural proteins responsible for muscle contraction, such as myosin and troponin, is also significantly reduced upon infection, particularly in the cardia inf+/- state (Fig 5A). Electron microscopy analysis also revealed a disorganization of the Z band of sarcomeres in muscle tissue surrounding the midgut epithelia in inf+/- cardia, but not in the control and inf+/+ cardia (Fig 5B-D). Extensive loss of muscle integrity was noted along the midgut epithelia in the inf+/- state. In addition, dilatation of the sarcoplasmic reticulum, muscle mitochondria swelling and vacuolation were observed, suggesting compromised muscle functions associated with this infection phenotype (S6 Fig). The detrimental effects of trypanosome infection on cardia structure and function are more apparent in the inf+/- compared to inf+/+ state, despite the higher number of parasites present during the latter phenotype (Fig 3D).

Oxidative stress restricts parasite infections in cardia inf+/-

Mitochondria produce reactive oxygen intermediates (ROIs) [29], which in excess can damage the organelle and surrounding cellular structures [30, 31]. The structural damage we observed in mitochondria, muscle tissue and fat cells of inf+/- cardia is symptomatic of oxidative stress [32]. Additionally, our EM observations demonstrate that parasites in inf+/- cardia exhibit cell-death

(Fig 6A-B), while parasites in inf+/+ cardia appear structurally intact (Fig 3E-F). Because ROIs modulates trypanosome infection outcomes in tsetse [15, 33], we hypothesized that ROIs may be responsible for controlling trypanosomes in inf +/- cardia and for producing an oxidative environment that concurrently results in tissue damage. We observed a significant increase of peroxide concentrations in both inf+/- (406nM; TukeyHSD posthoc test, $p<0.0001$) and inf+/+ (167nM; TukeyHSD posthoc test, $p=0.0008$) cardia relative to the control cardia (19 nM), with peroxide levels significantly higher in the inf+/- state (TukeyHSD posthoc test, $p<0.0001$) (Fig 6C). When we experimentally decreased oxidative stress levels in infected flies by supplementing their blood meal with the anti-oxidant cysteine (10µM) (Fig 6D), 85% of midgut infected flies developed SG infections, while only 45% of midgut infected flies had SG infections in the absence of the antioxidant (GLM, Wald-test $p<0.001$). Our results indicate that the significantly higher levels of ROIs produced in the inf+/- cardia may restrict parasite infections at this crucial junction, while lower levels of ROIs in the inf+/+ cardia may regulate the parasite density without impeding infection maintenance.

Homeostasis of redox balance is one of the most critical factors affecting host survival during continuous host-microbe interaction in the gastrointestinal tract [34]. In the mosquito *Anopheles gambiae*, increased mortality is observed when ROIs is produced in response to *Plasmodium berghei* infections [35]. A similar trade-off expressed in the inf+/- cardia may restrict parasite infections while causing collateral damage to essential physiologies. Conversely, strong anti-parasite responses that compromise essential physiologies are absent in infected cardia inf+/+, thus allowing the parasites to continue their journey to colonize the SG and successfully tranmit to a new host. Additionally, flies with SG parasite infections also suffer from longer feeding times due to suppressed anti-coagulation activity in the salivary glands, which may once again help with parasite transmission [36].

Conclusion

Trypanosome transmission by tsetse reflects a tug-of-war that begins with parasite colonization of the midgut and ends when parasites are transmitted to the next vertebrate via saliva. During the initial stages of infection establishment, BSF parasite surface antigens, VSGs, that are shed into the gut lumen have been found to manipulate vector gene expression in the cardia. This interference results in a transiently compromise PM that enables the parasites to escape the blood

bolus and invade the ES stage of the midgut. While tsetse's immune responses eliminate parasites from the majority of flies, some trypanosomes persist and colonize the cardia of a small proportion of flies. We show here that translocation from the cardia's ES to the lumen, by passing through the PM, is an integral component of the trypanosome life-cycle in tsetse and that loss of PM integrity is an essential requirement for the success of this process (summarized in Fig 7). Trypanosomes may once again manipulate this process by influencing the expression of PM-associated genes in the cardia through molecular interference, similar to what occurs in the initial stages of infection establishment in the midgut [9]. It is also possible that trypanosome produced products may further act on the PM to reduce its integrity and efficacy as a barrier. Finally, parasite transmission could represent a trade-off where vector tolerance to the parasites minimizes self-inflicted collateral damage. Our work substantiates the central role that the PM plays in the parasite-vector interaction. It potentializes this membrane as a target for vector control strategies to enhance its barrier function to block parasite transmission.

Methods

Ethical consideration

This work was carried out in strict accordance with the recommendations in the Office of Laboratory Animal Welfare at the National Institutes of Health and the Yale University Institutional Animal Care and Use Committee. The experimental protocol was reviewed and approved by the Yale University Institutional Animal Care and Use Committee (Protocol 2014-07266 renewed on May 2017).

Biological material

Glossina morsitans morsitans were maintained in Yale's insectary at 24°C with 50-55% relative humidity. All flies received defibrinated bovine blood (Hemostat Laboratories) every 48 hours through an artificial membrane feeding system. Only female flies were used in this study. Bloodstream form *Trypanosoma brucei brucei* (RUMP 503) were expanded in rats.

Flies were infected by supplementing the first blood meal of newly eclosed flies (teneral) with $5x10^6$ parasites /ml. Where mentioned, cysteine (10µM) was added to the infective blood meal to increase the infection prevalence [15].

For survival assays, *Serratia marcescens* strain Db11 was grown overnight in LB medium. Prior to supplementation with *Serratia*, the blood was inactivated by heat treatment at 56°C for 1 hour as described in [7].

mRNA Library Constructions and Sequencing

At day 40 post parasite challenge, all flies were dissected 48 hours after their last blood meal, and midgut and salivary glands (SG) were microscopically examined for infection status. Flies were classified as inf+/+ when infection was positive in both the midgut and the SG, as inf+/- when infection was positive in the midgut but negative in the SG. Cardia from inf+/+ and inf+/- flies were dissected and immediately placed in ice-cold TRIzol (Invitrogen). For each infected group, inf+/+ and inf+/-, 10 cardia were pooled into one biological replicate and three biological replicates were obtained and stored at -80°C prior to RNA extraction. Similarly, three biological replicates containing 10 cardia from age-matched flies that had only received normal blood meals (non-inf) were prepared. Total RNA was extracted from the nine biological replicates using the Direct-zol RNA Minipreps kit (Zymo Research) following the manufacturer instructions, then

subjected to DNase treatment using the Ambion TURBO DNA-free kit AM1907 (Thermo Fisher Scientific). RNA quality was analyzed using the Agilent 2100 Bioanalyzer RNA Nano chip. mRNA libraries were prepared using the NEBNext Ultra RNA Library Prep Kit for Illumina (New England BioLabs) following the manufacturer recommendations. The nine libraries were sequenced (single-end) at the Yale Center for Genome Analysis (YCGA) using the HiSeq2500 system (Illumina). Read files have been deposited in the NCBI BioProject database (ID# PRJNA358388).

RNA-seq data processing

Using CLC Genomics Workbench 8 (Qiagen), transcriptome reads were first trimmed and filtered to remove ambiguous nucleotides and low-quality sequences. The remaining reads were mapped to *Glossina morsitans morsitans* reference transcriptome GmorY1.5 (VectorBase.org). Reads aligning uniquely to *Glossina* transcripts were used to calculate differential gene expression using EdgeR package in R software [37].

Significance was determined using EdgeR exact test for the negative binomial distribution, corrected with a False Discovery Rate (FDR) at $P<0.05$.

Identified genes were functionally annotated by BlastX, with an E-value cut-off of $1e^{-10}$ and bit score of 200, and peptide data available from *D. melanogaster* database (FlyBase.org). Blast2GO was utilized to identify specific gene ontology (GO) terms that were enriched between treatments based on a Fisher's Exact Test [38].

Electron microscopy

Cardia tissues from non-inf, inf+/-, inf+/+ 40 day-old flies were dissected in 4% paraformaldehyde (PFA) and placed in 2.5% gluteraldehyde and 2% PFA in 0.1M sodium cacodylate buffer pH7.4 for 1 hour. Tissues were processed at the Yale Center for Cellular and Molecular Imaging (CCMI). Tissues were fixed in 1% osmium tetroxide, rinsed in 0.1M sodium cacodylate buffer and blocked and stained in 2% aqueous uranyl acetate for 1 hour. Subsequently, tissues were rinsed and dehydrated in a series in ethanol followed by embedment in resin infiltration Embed 812 (Electron Microscopy Sciences) and then stored overnight at 60°C. Hardened blocks were cut using a Leica UltraCut UC7 60nm. The resulting sections were collected on formvar/carbon coated grids and contrast-stained in 2% uranyl acetate and lead

409 citrate. Grids prepared from 3 different insects for each treatment were observed using a FEI
410 Tecnai Biotwin transmission electron microscope at 80Kv. Images were taken using a Morada
411 CCD camera piloted with the iTEM (Olympus) software.
412
413 **Quantification of trypanosomes**
414 At day 40 post parasite challenge, flies were dissected 72 hours after their last blood meal, and
415 midgut and salivary glands (SG) were microscopically examined for infection status. Cardia were
416 dissected, pooled by 5 in ice-cold TRIzol (Invitrogen) in function of their infection status (inf+/+
417 or inf+/-), and then flash-frozen in liquid nitrogen. RNA was extracted using the Direct-zol RNA
418 MiniPrep (Zymo Research) following the manufacturer instructions, then subjected to DNase
419 treatment using the Ambion TURBO DNA-free kit AM1907 (Thermo Fisher Scientific). 100ng
420 of RNA was utilized to prepare cDNA using the iScript cDNA synthesis kit (Bio-Rad) following
421 the manufacturer instructions. qPCR analysis was performed using SYBR Green supermix (Bio-
422 Rad) and a Bio-Rad C1000 thermal cycler. Quantitative measurements were performed in
423 duplicate for all samples. We used ATTCACGCTTTGGTTTGACC (forward) and
424 GCATCCGCGTCATTCATAA (reverse) as primers to amplify trypanosome *gapdh*. We used
425 CTGATTTCGTTGGTGATACT (forward) and CCAAATTCGTTGTCGTACCA (reverse) as
426 primers to amplify tsetse *gapdh*. Relative density of parasite was inferred by normalizing
427 trypanosome *gapdh* expression by tsetse *gapdh* expression. Statistical comparison of relative
428 densities was performed on Prism 7 (GraphPad software) using a Student t-test.
429 Direct counting of parasites was operated by dissecting the cardia and the whole remaining
430 midgut from flies prepared similarly than above. Individual tissues were homogenized in PSG
431 buffer (8 replicates for each tissue). Homogenate was then fixed in an equal volume of 4% PFA
432 for 30 min. The solution was then centrifuged 15 min at 1,000 rpm, the supernatant was discarded
433 and the pellets containing the trypanosomes from cardia and midguts were suspended in 100µl
434 and 2,500µl PSG buffer, respectively. Trypanosomes from the total solution were counted using a
435 hemocytometer. Statistical comparison of numbers was performed on Prism 7 (GraphPad
436 software) using a Mann-Whitney rank test.
437
438 **Midgut-associated procyclic trypanosome re-infection.**

At day 40 post parasite challenge, flies were dissected 72 hours after their last blood meal, and midgut and salivary glands (SG) were microscopically examined for infection status. Around 40 inf+/+ and inf+/- were independently pooled together, and then roughly homogenize in 500µl of PSG buffer (PBS+2% glucose). Each homogenate was centrifuged 10 min at 500 rpm to precipitate midgut debris, and then each supernatant containing parasites was transferred to a new tube to be centrifuged 15 min at 1,000 rpm to precipitate the parasites. Supernatants were then discarded and each pellet containing midgut procyclic trypanosomes either from inf+/+ or inf+/- flies was suspended in 500µl PSG. Parasites were counted using a hemocytometer.

Newly emerged adult females were provided a blood diet including 10 µM Cysteine and supplemented with 5×10^6 of procyclic trypanosomes from either inf+/+ or inf+/- flies prepared as described above. All flies were subsequently maintained on normal blood thereafter every 48 h. Four independent experiments were done for each type of trypanosomes. Midgut and salivary gland infections in each group were scored microscopically two weeks later. Precise sample sizes and count data are indicated in S3 Dataset.

Statistical analysis was carried out using the R software for macOS (version 3.3.2). A generalized linear model (GLM) was generated using binomial distribution with a logit transformation of the data. The binary infection status (inf+/+ or inf+/-) was analyzed as a function of the origin of the procyclic trypanosomes (inf+/+ or inf+/-) and the experiment it belongs to. The best statistical model was searched using a backward stepwise procedure from full additive model (*i.e.* parasite origin+experiment#) testing the main effect of each categorical explanatory factor. Using the retained model, we performed a Wald test on the individual regression parameters to test their statistical difference. Precise statistical results are indicated in S3 Dataset.

RNAi-mediated knockdown of PM-associated gene expression

Green fluorescent protein (*gfp*) and *chitin synthase* (*cs*) gene specific dsRNAs were prepared as described in [7]. Newly emerged adult females were provided with a trypanosome supplemented blood diet that also included 10 µM Cysteine. All flies were subsequently maintained on normal blood thereafter every 48 h. After 6 days (at the 3rd blood meal), flies were divided into two treatment groups: first group received dsRNA-*cs* and the second group control dsRNA-*gfp*. The dsRNAs were administered to each group in 3 consecutive blood meals containing 3mg dsRNA/20µl blood (the approximate volume a tsetse fly imbibes each time it feeds). Four

independent experiments using the same pool of dsRNA were generated for each treatment. Midgut and salivary gland infections in each group were scored microscopically three weeks later. Precise sample sizes and count data are indicated in S3 Dataset. Statistical analysis on the infection outcomes following the antioxidant feeding was carried out using the R software for macOS (version 3.3.2). A generalized linear model (GLM) was generated using binomial distribution with a logit transformation of the data. The binary infection status (inf+/+ or inf+/-) was analyzed as a function of the dsRNA treatment (dsRNA-*gfp* or dsRNA-*cs*) and the experiment it belongs to. The best statistical model was searched using a backward stepwise procedure from full additive model (*i.e.* dsRNA treatment+experiment#) testing the main effect of each categorical explanatory factors. Using the retained model, we performed a Wald test on the individual regression parameters to test their statistical difference. Precise statistical results are indicated in S3 Dataset.

Quantitative real-time PCR (qRT-PCR) was used to validate the effectiveness of our RNAi procedure as described in [7]. For each treatment of each experiment, we dissected the cardia of five randomly selected flies 72h after their third dsRNA-supplemented blood meal. The five dissected cardia were pooled together and their RNA was extracted. 100ng RNA was used to generate cDNA. RNA extractions from experiment #3 failed, but as the same dsRNA pools were used for all experiments and considering the consistency of the knockdown we observed, we decided to maintain experiment #3 in our counting results.

***Serratia* infection assay to assess peritrophic matrix integrity**

To assess the PM integrity, we applied a host survival assay following *per os* treatment of each group with *Serratia marcescens* as described in [7, 9]. We provided to three groups of 8 day-old flies (in their 4th blood meal) either cardia extracts obtained from challenged flies that cleared the trypanosomes and are subsequently recovered from initial infection (rec-/-), or a cardia extract from inf+/- flies, or a cardia extract from inf+/+ flies. We included a fourth group of 8-day old flies that received an untreated blood meal.

Cardia extract was obtained by dissecting, in PBS, the cardia from 40 days-old infected as described above. Approximately fifty cardia from either rec-/-, inf+/- or inf+/+ flies were pooled together, and then gently homogenized. Parasites were counted from the homogenates of inf+/- and inf+/+ using a hemocytometer. The three cardia homogenates were then heated at 100°C for

10 minutes. inf+/- and inf+/+ extracts were provided to reach a concentration of 5×10^5 parasites per ml of blood. As inf+/- cardia contain fewer parasites than inf+/+ cardia, the volume of the inf+/+ extract provided was adjusted by dilution in PSG buffer to be equal to inf+/- volume. Rec-/- extract was provided at an equal volume than infected extracts to ensure the presence of a similar quantity of extract molecules coming from the cardia in these groups. 48 hours after the flies received blood meal supplemented with the different extracts, all flies were provided a blood meal supplemented with 1,000 CFU/ml of *S. marcescens* strain Db11. Thereafter, flies were maintained on normal blood every other day, while their mortality was recorded every day for 30 days. Precise counting data are indicated in S3 Dataset.

Statistical analysis was carried out using the R software for macOS (version 3.3.2). We used an accelerated failure time model (Weibull distribution) where survival was analyzed as a function of the extract received (survreg() function of "survival" package). Pairwise tests were generated using Tukey contrasts on the survival model (glht() function of "multcomp" package). Precise statistical results are indicated in S3 Dataset.

Antioxidant feeding

Newly emerged adult females were provided with a trypanosome-supplemented blood diet that also included 10 µM Cysteine. All flies were subsequently maintained on normal blood thereafter every 48 h. After 10 days (at the 5th blood meal), flies were divided into two treatment groups: first group received the anti-oxidant Cysteine (10µM) and the second group was fed normally as a control. Cysteine was administered each blood meal until dissection. Four independent experiments were done for each treatment. Midgut and salivary gland infections in each group were scored microscopically three weeks later. Precise sample sizes and count data are indicated in S3 Dataset.

Statistical analysis was carried out using the R software for macOS (version 3.3.2). A generalized linear model (GLM) was generated using binomial distribution with a logit transformation of the data. The binary infection status (inf+/+ or inf+/-) was analyzed as a function of the treatment (control or cysteine) and the experiment it belongs to. The best statistical model was searched using a backward stepwise procedure from full additive model (*i.e.* antioxidant treatment+experiment#) testing the main effect of each categorical explanatory factors. Using the

retained model, we performed a Wald test on the individual regression parameters to test their statistical difference. Precise statistical results are indicated in S3 Dataset.

Quantification of reactive oxygen species (ROS) in cardia tissues

ROS were quantified using the Amplex Red Hydrogen Peroxide/Peroxidase Assay Kit (ThermoFisher Scientific), following the manufacturer recommendations. 40 days post parasite challenge, flies were dissected 72 hours after their last blood meal, and midgut and salivary glands (SG) were microscopically examined for infection status. For each infection phenotype (i.e. inf+/+ or inf+/-), 3 replicates containing each 10 cardia tissues pooled and homogenized in 80µl of ice-cold Amplex Red Kit 1X Reaction Buffer were generated. 3 replicates of age-matched non-infected cardia tissues were conceived in the same manner. 50µl of assay reaction mix was added to 50µl of the supernatant of each samples, and then incubated 60 minutes at RT. Fluorescence units were determined using a BioTek Synergy HT plate reader (530nm excitation; 590nm emission). Peroxide concentrations were determined using the BioTek Gen5 software calculation inferred from a standard curve (precise results are indicated in S3 Dataset). Statistical analysis was performed on Prism 7 (GraphPad software) using a one-way ANOVA where ROS concentration was analyzed as a function of the infection status. Pairwise comparisons were carried out using a TukeyHSD posthoc test.

549 ## Acknowledgements

550 We thank Dr. Ying Yang for technical assistance with the tsetse fly colony, Drs. Nikolay Kolev
551 and Chris Tschudi for their advice with data interpretation, Morven Graham for her assistance
552 with electron microscopy data interpretation, and Drs. Maria Onyango, Mehmet Karakus and
553 Florent Masson for their critical comments on the manuscript.

554

References

1. Simarro PP, Cecchi G, Franco JR, Paone M, Diarra A, Priotto G, et al. Monitoring the progress towards the elimination of gambiense human African trypanosomiasis. PLOS Negl Trop Dis. 2015;9(6):e0003785. Epub 2015/06/10. doi: 10.1371/journal.pntd.0003785. PubMed PMID: 26056823; PubMed Central PMCID: PMCPMC4461311.

2. Simarro PP, Cecchi G, Franco JR, Paone M, Diarra A, Ruiz-Postigo JA, et al. Estimating and mapping the population at risk of sleeping sickness. PLOS Negl Trop Dis. 2012;6(10):e1859. Epub 2012/11/13. doi: 10.1371/journal.pntd.0001859. PubMed PMID: 23145192; PubMed Central PMCID: PMCPMC3493382.

3. Courtin F, Camara M, Rayaisse JB, Kagbadouno M, Dama E, Camara O, et al. Reducing human-tsetse contact significantly enhances the efficacy of sleeping sickness active screening campaigns: a promising result in the context of elimination. PLOS Negl Trop Dis. 2015;9(8):e0003727. Epub 2015/08/13. doi: 10.1371/journal.pntd.0003727. PubMed PMID: 26267667; PubMed Central PMCID: PMCPMC4534387.

4. Davis S, Aksoy S, Galvani A. A global sensitivity analysis for African sleeping sickness. Parasitology. 2011;138(4):516-26. Epub 2010/11/17. doi: 10.1017/S0031182010001496. PubMed PMID: 21078220; PubMed Central PMCID: PMCPMC3282146.

5. Hegedus D, Erlandson M, Gillott C, Toprak U. New insights into peritrophic matrix synthesis, architecture, and function. Annu Rev Entomol. 2009;54:285-302. Epub 2008/12/11. doi: 10.1146/annurev.ento.54.110807.090559. PubMed PMID: 19067633.

6. Rose C, Belmonte R, Armstrong SD, Molyneux G, Haines LR, Lehane MJ, et al. An investigation into the protein composition of the teneral *Glossina morsitans morsitans* peritrophic matrix. PLOS Negl Trop Dis. 2014;8(4):e2691. Epub 2014/04/26. doi: 10.1371/journal.pntd.0002691. PubMed PMID: 24763256; PubMed Central PMCID: PMCPMC3998921.

7. Weiss BL, Savage AF, Griffith BC, Wu Y, Aksoy S. The peritrophic matrix mediates differential infection outcomes in the tsetse fly gut following challenge with commensal, pathogenic, and parasitic microbes. J Immunol. 2014;193(2):773-82. Epub 2014/06/11. doi: 10.4049/jimmunol.1400163. PubMed PMID: 24913976; PubMed Central PMCID: PMCPMC4107339.

8. Rodgers FH, Gendrin M, Wyer CAS, Christophides GK. Microbiota-induced peritrophic matrix regulates midgut homeostasis and prevents systemic infection of malaria vector mosquitoes. PLOS Pathog. 2017;13(5):e1006391. Epub 2017/05/26. doi: 10.1371/journal.ppat.1006391. PubMed PMID: 28545061; PubMed Central PMCID: PMCPMC5448818.

9. Aksoy E, Vigneron A, Bing X, Zhao X, O'Neill M, Wu YN, et al. Mammalian African trypanosome VSG coat enhances tsetse's vector competence. Proc Natl Acad Sci U S A. 2016;113(25):6961-6. Epub 2016/05/18. doi: 10.1073/pnas.1600304113. PubMed PMID: 27185908; PubMed Central PMCID: PMCPMC4922192.

10. Coutinho-Abreu IV, Sharma NK, Robles-Murguia M, Ramalho-Ortigao M. Characterization of *Phlebotomus papatasi* peritrophins, and the role of PpPer1 in *Leishmania* major survival in its natural vector. PLOS Negl Trop Dis. 2013;7(3):e2132. Epub 2013/03/22. doi:

10.1371/journal.pntd.0002132. PubMed PMID: 23516661; PubMed Central PMCID: PMCPMC3597473.

11. Narasimhan S, Rajeevan N, Liu L, Zhao YO, Heisig J, Pan J, et al. Gut microbiota of the tick vector *Ixodes scapularis* modulate colonization of the Lyme disease spirochete. Cell Host Microbe. 2014;15(1):58-71. Epub 2014/01/21. doi: 10.1016/j.chom.2013.12.001. PubMed PMID: 24439898; PubMed Central PMCID: PMCPMC3905459.

12. Turner CM, Barry JD, Vickerman K. Loss of variable antigen during transformation of *Trypanosoma brucei rhodesiense* from bloodstream to procyclic forms in the tsetse fly. Parasitol Res. 1988;74(6):507-11. Epub 1988/01/01. PubMed PMID: 3194363.

13. Hao Z, Kasumba I, Lehane MJ, Gibson WC, Kwon J, Aksoy S. Tsetse immune responses and trypanosome transmission: implications for the development of tsetse-based strategies to reduce trypanosomiasis. Proc Natl Acad Sci U S A. 2001;98(22):12648-53. Epub 2001/10/11. doi: 10.1073/pnas.221363798. PubMed PMID: 11592981; PubMed Central PMCID: PMCPMC60108.

14. Hu Y, Aksoy S. An antimicrobial peptide with trypanocidal activity characterized from *Glossina morsitans morsitans*. Insect Biochem Mol Biol. 2005;35(2):105-15. Epub 2005/02/01. doi: 10.1016/j.ibmb.2004.10.007. PubMed PMID: 15681221.

15. MacLeod ET, Maudlin I, Darby AC, Welburn SC. Antioxidants promote establishment of trypanosome infections in tsetse. Parasitology. 2007;134(Pt 6):827-31. Epub 2007/02/20. doi: 10.1017/S0031182007002247. PubMed PMID: 17306056.

16. Wang J, Aksoy S. PGRP-LB is a maternally transmitted immune milk protein that influences symbiosis and parasitism in tsetse's offspring. Proc Natl Acad Sci U S A. 2012;109(26):10552-7. Epub 2012/06/13. doi: 10.1073/pnas.1116431109. PubMed PMID: 22689989; PubMed Central PMCID: PMCPMC3387098.

17. Haines LR, Lehane SM, Pearson TW, Lehane MJ. Tsetse EP protein protects the fly midgut from trypanosome establishment. PLOS Pathog. 2010;6(3):e1000793. Epub 2010/03/12. doi: 10.1371/journal.ppat.1000793. PubMed PMID: 20221444; PubMed Central PMCID: PMCPMC2832768.

18. Sharma R, Peacock L, Gluenz E, Gull K, Gibson W, Carrington M. Asymmetric cell division as a route to reduction in cell length and change in cell morphology in trypanosomes. Protist. 2008;159(1):137-51. Epub 2007/10/13. doi: 10.1016/j.protis.2007.07.004. PubMed PMID: 17931969.

19. Van Den Abbeele J, Claes Y, van Bockstaele D, Le Ray D, Coosemans M. *Trypanosoma brucei* spp. development in the tsetse fly: characterization of the post-mesocyclic stages in the foregut and proboscis. Parasitology. 1999;118 (Pt 5):469-78. Epub 1999/06/11. PubMed PMID: 10363280.

20. Buxton P. The natural history of tsetse flies. London: H. K. Lewis and Co. Ltd.; 1955.

21. Lehane MJ. Peritrophic matrix structure and function. Annu Rev Entomol. 1997;42:525-50. Epub 1997/01/01. doi: 10.1146/annurev.ento.42.1.525. PubMed PMID: 15012322.

22. Wigglesworth VB. Digestion in the tsetse-fly: a study of structure and function. Parasitology. 1929;21(3):288-321.

23. Hao Z, Aksoy S. Proventriculus-specific cDNAs characterized from the tsetse, *Glossina morsitans morsitans*. Insect Biochem Mol Biol. 2002;32(12):1663-71. Epub 2002/11/14. PubMed PMID: 12429118.

24. Gibson W, Bailey M. The development of *Trypanosoma brucei* within the tsetse fly midgut observed using green fluorescent trypanosomes. Kinetoplastid Biol Dis. 2003;2(1):1. Epub 2003/05/29. PubMed PMID: 12769824; PubMed Central PMCID: PMCPMC156611.

25. Schuster S, Krüger T, Subota I, Thusek S, Rotureau B, Beilhack A, et al. Developmental adaptations of trypanosome motility to the tsetse fly host environments unravel a multifaceted *in vivo* microswimmer system. eLife. 2017;6:e27656. doi: 10.7554/eLife.27656.

26. Kuraishi T, Binggeli O, Opota O, Buchon N, Lemaitre B. Genetic evidence for a protective role of the peritrophic matrix against intestinal bacterial infection in *Drosophila melanogaster*. Proc Natl Acad Sci U S A. 2011;108(38):15966-71. Epub 2011/09/08. doi: 10.1073/pnas.1105994108. PubMed PMID: 21896728; PubMed Central PMCID: PMCPMC3179054.

27. Oberholzer M, Lopez MA, McLelland BT, Hill KL. Social motility in African trypanosomes. PLOS Pathog. 2010;6(1):e1000739. Epub 2010/02/04. doi: 10.1371/journal.ppat.1000739. PubMed PMID: 20126443; PubMed Central PMCID: PMCPMC2813273.

28. Imhof S, Knusel S, Gunasekera K, Vu XL, Roditi I. Social motility of African trypanosomes is a property of a distinct life-cycle stage that occurs early in tsetse fly transmission. PLOS Pathog. 2014;10(10):e1004493. Epub 2014/10/31. doi: 10.1371/journal.ppat.1004493. PubMed PMID: 25357194; PubMed Central PMCID: PMCPMC4214818.

29. Murphy MP. How mitochondria produce reactive oxygen species. Biochem J. 2009;417(1):1-13. Epub 2008/12/09. doi: 10.1042/BJ20081386. PubMed PMID: 19061483; PubMed Central PMCID: PMCPMC2605959.

30. Kowaltowski AJ, Vercesi AE. Mitochondrial damage induced by conditions of oxidative stress. Free Radic Biol Med. 1999;26(3-4):463-71. Epub 1999/01/23. PubMed PMID: 9895239.

31. Wang Y, Nartiss Y, Steipe B, McQuibban GA, Kim PK. ROS-induced mitochondrial depolarization initiates PARK2/PARKIN-dependent mitochondrial degradation by autophagy. Autophagy. 2012;8(10):1462-76. Epub 2012/08/15. doi: 10.4161/auto.21211. PubMed PMID: 22889933.

32. Bravard A, Bonnard C, Durand A, Chauvin MA, Favier R, Vidal H, et al. Inhibition of xanthine oxidase reduces hyperglycemia-induced oxidative stress and improves mitochondrial alterations in skeletal muscle of diabetic mice. Am J Physiol Endocrinol Metab. 2011;300(3):E581-91. Epub 2011/01/13. doi: 10.1152/ajpendo.00455.2010. PubMed PMID: 21224483.

33. Ridgley EL, Xiong ZH, Ruben L. Reactive oxygen species activate a Ca2+-dependent cell death pathway in the unicellular organism *Trypanosoma brucei brucei*. Biochem J. 1999;340 (Pt 1):33-40. Epub 1999/05/07. PubMed PMID: 10229656; PubMed Central PMCID: PMCPMC1220219.

34. Ha EM, Oh CT, Ryu JH, Bae YS, Kang SW, Jang IH, et al. An antioxidant system required for host protection against gut infection in Drosophila. Dev Cell. 2005;8(1):125-32. Epub 2004/12/29. doi: 10.1016/j.devcel.2004.11.007. PubMed PMID: 15621536.

35. Molina-Cruz A, DeJong RJ, Charles B, Gupta L, Kumar S, Jaramillo-Gutierrez G, et al. Reactive oxygen species modulate *Anopheles gambiae* immunity against bacteria and *Plasmodium*. J Biol Chem. 2008;283(6):3217-23. Epub 2007/12/11. doi: 10.1074/jbc.M705873200. PubMed PMID: 18065421.

683 36. Van Den Abbeele J, Caljon G, De Ridder K, De Baetselier P, Coosemans M. *Trypanosoma*
684 *brucei* modifies the tsetse salivary composition, altering the fly feeding behavior that favors
685 parasite transmission. PLOS Pathog. 2010;6(6):e1000926. Epub 2010/06/10. doi:
686 10.1371/journal.ppat.1000926. PubMed PMID: 20532213; PubMed Central PMCID:
687 PMCPMC2880569.
688 37. Robinson MD, McCarthy DJ, Smyth GK. edgeR: a Bioconductor package for differential
689 expression analysis of digital gene expression data. Bioinformatics. 2010;26(1):139-40. Epub
690 2009/11/17. doi: 10.1093/bioinformatics/btp616. PubMed PMID: 19910308; PubMed Central
691 PMCID: PMCPMC2796818.
692 38. Conesa A, Gotz S, Garcia-Gomez JM, Terol J, Talon M, Robles M. Blast2GO: a universal
693 tool for annotation, visualization and analysis in functional genomics research. Bioinformatics.
694 2005;21(18):3674-6. Epub 2005/08/06. doi: 10.1093/bioinformatics/bti610. PubMed PMID:
695 16081474.
696

Figure captions

Fig 1. Dynamics of parasite infection in tsetse flies.

(A) Cardia and SG organs were dissected from 40-day old female flies subjected to a single parasite infection as newly eclosed adults. Infection prevalence data for infected cardia (white circles) and infected salivary glands (grey circles) are shown for three independent replicate experiments. The black bars represent the mean of the three replicates. The total number of flies used for the 3 biological samples is: N_1=46; N_2=71; N_3=73. **(B)** Localization of trypanosomes in tsetse fly tissues. In the non-permissive flies (inf+/- state, shown in the upper scheme) only the midgut, including the cardia, is colonized by parasites, which reside in the ectoperitrophic space (purple). In the permissive flies (inf+/+ state, shown the lower scheme), in addition to being located in the midgut, parasites colonize the SG (violet). **(C)** Percentage of permissive infections (inf+/+) following challenge at teneral stage with procyclic parasites obtained from either inf+/- or inf+/+ midgut. A total of 4 experiments were performed for each treatment. A total number of 64 infected flies were observed for each treatment. The black bar represents the mean of the 4 experiments. SG infection is independent of the initial inf+/- or inf+/+ status of the parasite used for fly infection (GLM, p=1, detailed model in S3 Dataset).

Fig 2. **Trypanosome infection establishment process**

(A) Percentage of RNAseq reads mapped to the parasite reference geneset from the three biological replicates of inf+/- cardia is depicted in red circles and inf+/+ depicted in blue circles. A same number in the circle depict flies from the same sample. The total number of flies used for the 3 biological samples is: N_1=46; N_2=71; N_3=73. The black bars indicate the mean of the 3 replicates. (**B)** Abundance of trypanosome *gapdh* relative to tsetse *gapdh* determined from inf+/- cardia (shown by red circles) and inf+/+ cardia (shown by blue circles). The black bars indicate the mean of the replicates. The increase in relative abundance indicates an increase in parasite numbers in the inf+/+ cardia (Student t-test, p= 0.0028). (**C)** Schematic representation of the cardia organ based on microscopic observations. The cardia is composed of cells originating from the foregut (light orange) and midgut (light blue) at the junction of the fore- and mid-gut. The midgut cells form a glandular tissue that secretes the PM components are shown in green along with the foregut opposing cells. Sphincter muscles that form a ring above the glandular cells are indicated as well as the thin layer of muscle that surrounds large lipid-containing cells (shown in

yellow). (**D-E)** Electron microscopy observations of trypanosomes within cardia inf+/- (D) and cardia inf+/+ (E).

Fig 3. Parasite infection effects on PM synthesis in cardia inf+/+ and inf+/-

(A) Percentage of the total transcriptome expression represented by PM-associated transcripts. (**B)** Differential expression of PM-associated transcripts in flies that present distinct infection phenotypes. Each dot represents the abundance of one transcript expressed as fold-change against the non-infected control. The expression values from infected +/+ cardia are shown by blue circles and from infected +/- cardia as red circles. The grey area delimits fold-changes that are <1.5, statistically not different from the control cardia ($p > 0.05$ after FDR correction). For each data point, the *Glossina* gene ID and function based on BlastX annotation is depicted on the x-axis. (**C)** SG infection prevalence in normal and PM compromised flies. The circles depict the percentage of flies that harbor both gut and SG infections in the dsRNA-*chitin synthase* (dsCS) and control dsRNA-*gfp* (dsGFP) treatment groups. A total of 4 independent experiments were set-up for both dsGFP and dsCS. The black bars indicate the mean of the 4 experiments. A total number of 66 and 63 infected flies were observed in the dsGFP and dsCS treatments, respectively. The dsCS treatment significantly increases trypanosome infection prevelance in tsetse's salivary glands (GLM, Wald-test $p=0.01408$). Detailed countings and a complete statistical model are indicated in S3 Dataset. (**D)** Effects of cardia inf+/- and inf+/+ extracts on PM integrity. Survival of flies was followed daily after *per os* treatment of 8 day-old flies with cardia extracts followed by *per os* treatment with *Serratia marcescens* 72 hours later. The Kaplan-Meyer curves show fly survival over time: cardia inf+/- (red), cardia inf+/+ (blue), or cardia rec-/- (green) and cardia non-inf (black). Statistical analysis was performed using a full regression model followed by a pairwise test (details in S3 Dataset). Different letters next to figure legends represent significantly different curves ($p < 0.05$). (**E-F)** Electron microscopy observations of trypanosomes within cardia inf+/+. (E) Trypanosomes accumulate where the foregut and midgut join and synthesize the PM. At this point, the PM is very diffused, which may facilitate parasites passage out of the ES. (F) The peritrophic matrix (PM) is ruptured (star) where trypanosomes aggregate as a cyst-like body. Tryp.: trypanosomes; ES: ectoperitrophic space; mv: midgut microvilli.

Fig 4. Mitochondrial integrity in cardia inf+/+ and inf+/-

(A) Effect of infection on mitochondria related gene expression. Heatmap generated from the fold-changes between control and either inf+/- or inf+/+ cardia. The * denote the level of significance associated with the DE of specific transcripts (*p<0.05; **p<0.01; ***p<0.001; ****p<0.0001). (**B-D)** Ultrastructure of the sphincter myofibrils in control non-inf (B), inf+/- (C) and inf+/+ (D) cardia. The white arrows show the mitochondria, the red arrowheads show patterns of mitochondria degradation and the yellow arrows show dilatation of sarcoplasmic reticulum. (**E-G)** Ultrastructure of the giant lipid-containing cells control non-inf (E), inf+/- (F) and inf+/+ (G) cardia. The white arrows show the mitochondria and Ld denotes lipid droplets, Nu denotes nucleus. In both infection phenotypes, mitochondria cristae appear disogarnized compared to control.

Fig 5. Muscle structural integrity in cardia inf+/+ and inf+/-

(A) Effect of infection on cardia muscle related gene expression. Heatmap generated from the fold-changes between control and either inf+/- or inf+/+ cardia. The * denote the level of significance associated with the DE of specific transcripts (*p<0.05; **p<0.01; ***p<0.001; ****p<0.0001). (**B-D)** Ultrastructure of a sarcomere of muscles surrounding non-inf (B), inf+/- (C) and inf+/+ (D) cardia. The red arrowhead indicates the Z band structure associated with sarcomeres.

Fig 6. Influence of oxidative stress on infection status

(A-B) Electron microscopy observations of trypanosomes within cardia inf+/-. (C) Comparison of peroxide levels in cardia non-infected (white circles), inf+/- (red circles) and inf+/+ (blue circles) 72 hours after a blood meal. Each dot represents an independent quantification of 10 pooled cardia. The black bars indicate the mean of the 3 replicates. Statistical analysis was conducted using a one-way ANOVA followed by a TukeyHSD posthoc test for pairwise comparisons. Statistical significance is represented by letters above each condition, with different letters indicating distinct statistical groups (p< 0.05). **(D)** SG infection prevalence in normal and anti-oxidant treated flies. The circles depict the percentage of flies that harbor both gut and SG infections in the Cysteine (10µM) and control treatment groups. A total of 4 independent groups were set-up for each treatment. The black bars indicate the mean of the 4 experiments. A total

number of 91 and 89 infected flies were observed in the control and Cysteine treatments, respectively. Cysteine treatment significantly increases trypanosome infection prevelance in tsetse's salivary glands (GLM, Wald-test $p<0.001$). Detailed countings and complete statistical model are indicated in S3 Dataset.

Fig 7. Model illustrating permissive (inf+/+) and non-permissive (inf+/-) infection phenotypes in tsetse's cardia.

African trypanosomes must pass through the tsetse vector in order to complete their lifecycle and infect a new vertebrate host. Following infection of tsetse's midgut, parasites either migrate to the fly's salivary glands where they subsequently transmit (permissive infection), or remain trapped in this environment and fail to advance (non-permissive infection). For a permissive infection to occur (inf+/+), trypanosomes must successfully circumvent several immunological barriers, including the cardia-synthesized peritrophic matrix (PM). In this situation, parasites that have accumulated in the ectoperitrophic space (ES) (1) of the cardia traverse the structurally compromised PM at its site of synthesis (where the matrix is most diffuse and fragile) (2). During this process, clumps of parasites end up enclosed within layers of the PM, but force their way out by breaking through the structure's electron-dense layer (3). Parasites that have successfully translocated to the cardia lumen then migrate to tsetse's salivary glands (4). Why the PM is structurally compromised in the permissive state is currently unknown. However, trypanosomes may secrete molecules that are taken up by PM synthesizing cells (5). These molecules may subsequently inhibit expression of genes that encode proteinaceous components (Pro1, Pro3, etc) of the matrix and trypanocidal reactive oxygen intermediates (ROIs). In non-permissive infection (inf+/-), a small number of parasites are found to have successfully reach the cardia, and most of them appear dead or damaged (6). The inability for the parasite to sustain in the cardia environment seems caused by a higher concentration of ROIs compared to inf+/+ cardia. The regulation of the parasite population comes at the price of collateral damages to the cardia tissues, especially to the muscles lining the outer boarder of the organ, as they present sarcoplasmic dilatation and mitochondrial vacuolation and swelling (7). In the cardia with non-permissive phenotype, PM synthesis is not affecting, probably due to the lack of trypanosome-derived molecules interfering with its production (8).

Supporting Information

S1 Fig. Overview of cardia transcriptomes. (A) For each replicate of each infection status, number of RNA-seq reads: in total (blue), after quality control (purple), mapping uniquely to tsetse *Glossina morsitans morsitans* (bright red), mapping non-uniquely to tsetse *Glossina morsitans morsitans* (pale red), mapping uniquely to *Trypanosoma brucei brucei* 927 (dark green), mapping non-uniquely to *Trypanosoma brucei brucei* 927 (bright green). **(B)** Proportion of total trimmed reads mapping to Glossina morsitans morsitans uniquely (bright red) and non-uniquely (pale red) and mapping to Trypanosoma brucei brucei 927 uniquely (dark green) and non-uniquely (bright green). **(C)** Proportion of *Glossina morsitans morsitans* transcripts for which 0-1,000 (blue), 1,001-10,000 (yellow), 10,001-100,000 (pink) or 100,001+ (purple) reads are mapping to.

S2 Fig. Parasite quantity in midgut and cardia. (A) Number of parasites in the cardia of inf+/- (red) and inf+/+ (blue) flies. **(B)** Number of parasites in the midgut of inf+/- (red) and inf+/+ (blue) flies. The black bar represents the mean of the replicates for each treatment. Midgut and cardia were dissected from eight 40 days-old females. Parasites were counted using a hemocytometer. Statistical analyses were carried out using the non-parametrical Mann-Whitney rank test.

S3 Fig. Ultrastructure of the cardia. (A) Transversal section of a non-infected cardia. Two pictures of the same cardia were merged to produce a larger picture. B, C, D, E and F locate the magnification of cardia tissues. **(B)** Midgut tissue delimiting the outer part of the cardia. **(C)** Foregut tissue invagination within cardia, corresponding to the stomodeal valve in other insects. **(D)** Myofibrils assembled to form the sphincter surrounding the foregut opening in the cardia. **(E)** Lipid-containing cells above foregut tissue and cover by a thin layer of muscles. **(F)** Foregut tube coming out of the cardia. Lu, Lumen; Mg, Midgut; S-Mg, PM-Secreting part of Midgut; Fg, Foregut; mu, muscle; Lc, Lipid-containing cells; mv, microvilli; ES, Ecotperitrophic Space.

S4 Fig. Expression of *chitin synthase* after RNAi treatment. Expression of *chitin synthase* gene relative to the expression of the housekeeping gene *ß-tubulin* after treatment with dsRNA-

gfp (control; white circles) and dsRNA-*chitin synthase* (dsCS; grey circles). *chitin synthase* expression is significantly decreased after RNAi knockdown (Student t-test, $p = 0.011$).

S5 Fig. Ultrastructure of trypanosomes aggregations in inf+/+ cardia. (A) Aggregation of trypanosomes in-between the foregut invagination (characterized by its chitin layer) and the midgut (characterized by the microvilli, mv) below the site of the PM synthesis. The compact aggregate of parasite is observed in the lumen as well as in the ectoperitrophic space (ES). **(B)** Close-up of the A panel where the PM appears as compressed in-between parasites. **(C)** Formation of a cyst-like body at the site of the PM synthesis. Here, the PM appears very diffused, which may be exploited by the parasites to evade the ES. **(D)** Cyst-like bodies are observed at several points in the cardia, where parasites are enclosed in-between 2 distinguishable PM layers: a thick electron-lucent part on the ES side and a thin electron-dense part on the lumen side. The electron-dense layer appears broken at some points (arrowhead, see also Fig 3F), where parasites may evade from the PM. **(E)** Rupture of the PM electron-dense layer are also observed along the PM in the cardia (arrowhead). This may be the result of parasites cyst-like bodies that have successfully escape the PM. **(F)** The PM lacks its electron-dense layer on some portion longing the cardia midgut epithelium, resulting presumably from the event describe above.

S6 Fig. Ultrastructure of muscles and mitochondria damages in cardia inf+/-. (A) Transversal section of muscle tissues (mu) composing the sphincter. **(B-D)** Longitudinal section of muscles (mu) layering the midgut tissues. Black arrowheads: healthy mitochondria; red arrowheads: vacuolation of mitochondria; yellow arrow: sarcoplasmic dilatation; green arrowheads: swelling mitochondria.

S1 Dataset. Detailed results and analyses fo each transcriptome.

S2 Dataset. GO terms analysis results.

S3 Dataset. Detailed results and statistics for infection experiments and oxidative stress quantification.

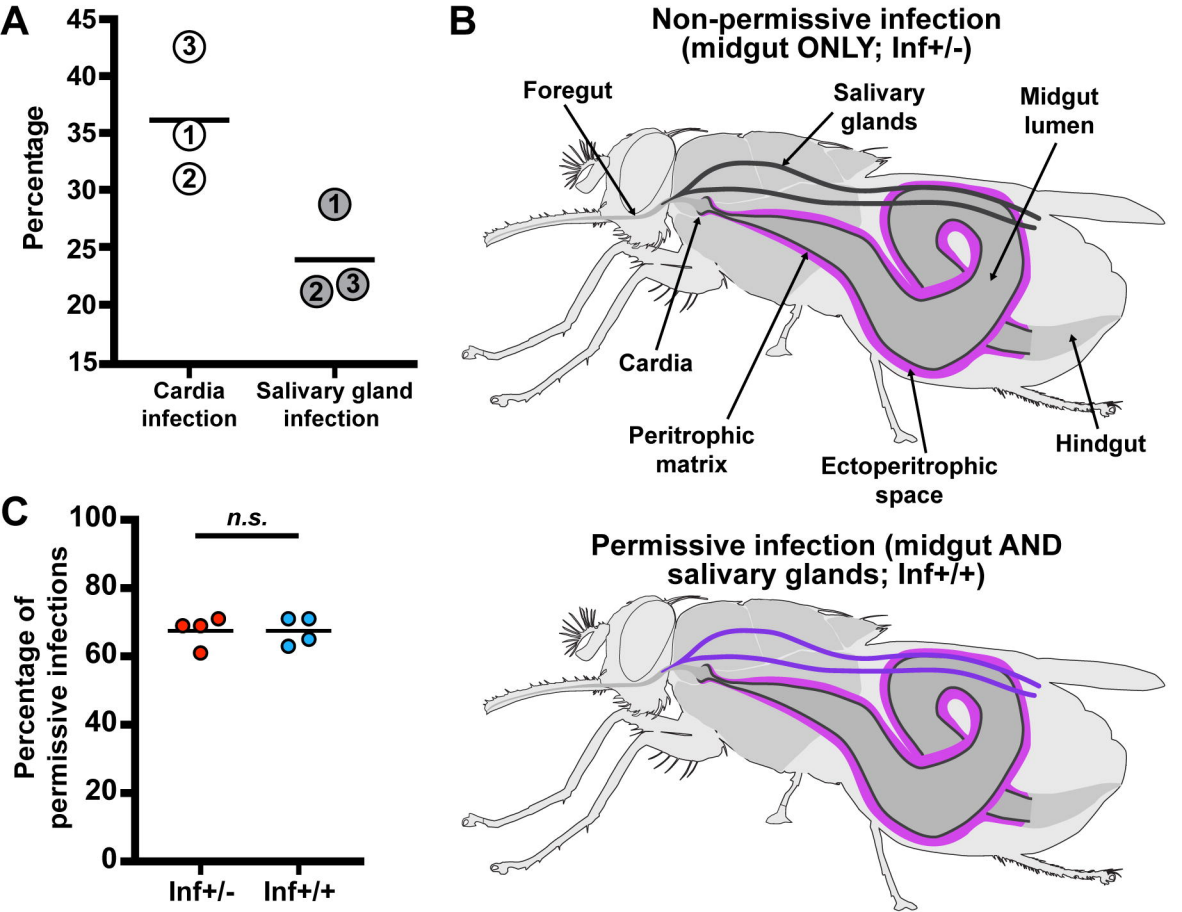
A
Percentage
45
40
35
30
25
20
15
3
1
2
1
2
3
Cardia infection
Salivary gland infection
B
Non-permissive infection (midgut ONLY; Inf+/-)
Foregut
Salivary glands
Midgut lumen
Cardia
Peritrophic matrix
Ectoperitrophic space
Hindgut
C
Percentage of permissive infections
100
80
60
40
20
0
n.s.
Inf+/-
Inf+/+
Permissive infection (midgut AND salivary glands; Inf+/+)

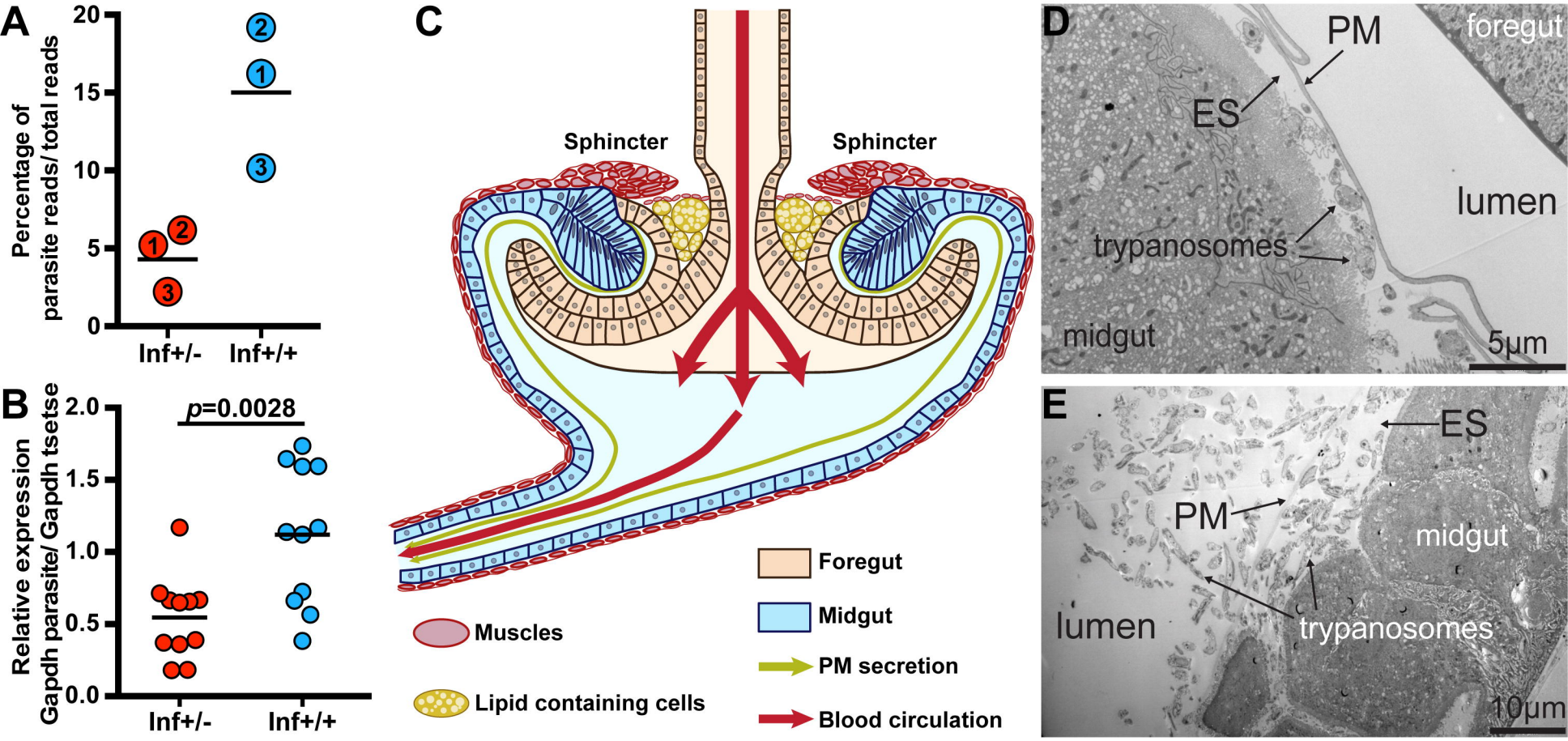
A
Percentage of parasite reads/ total reads
20
15
10
5
0
Inf+/-
Inf+/+
B
Relative expression Gapdh parasite/ Gapdh tsetse
p=0.0028
2.0
1.5
1.0
0.5
0.0
Inf+/-
Inf+/+
C
Sphincter
Sphincter
Foregut
Midgut
Muscles
PM secretion
Lipid containing cells
Blood circulation
D
PM
foregut
ES
lumen
trypanosomes
midgut
5µm
E
ES
PM
midgut
lumen
trypanosomes
10µm

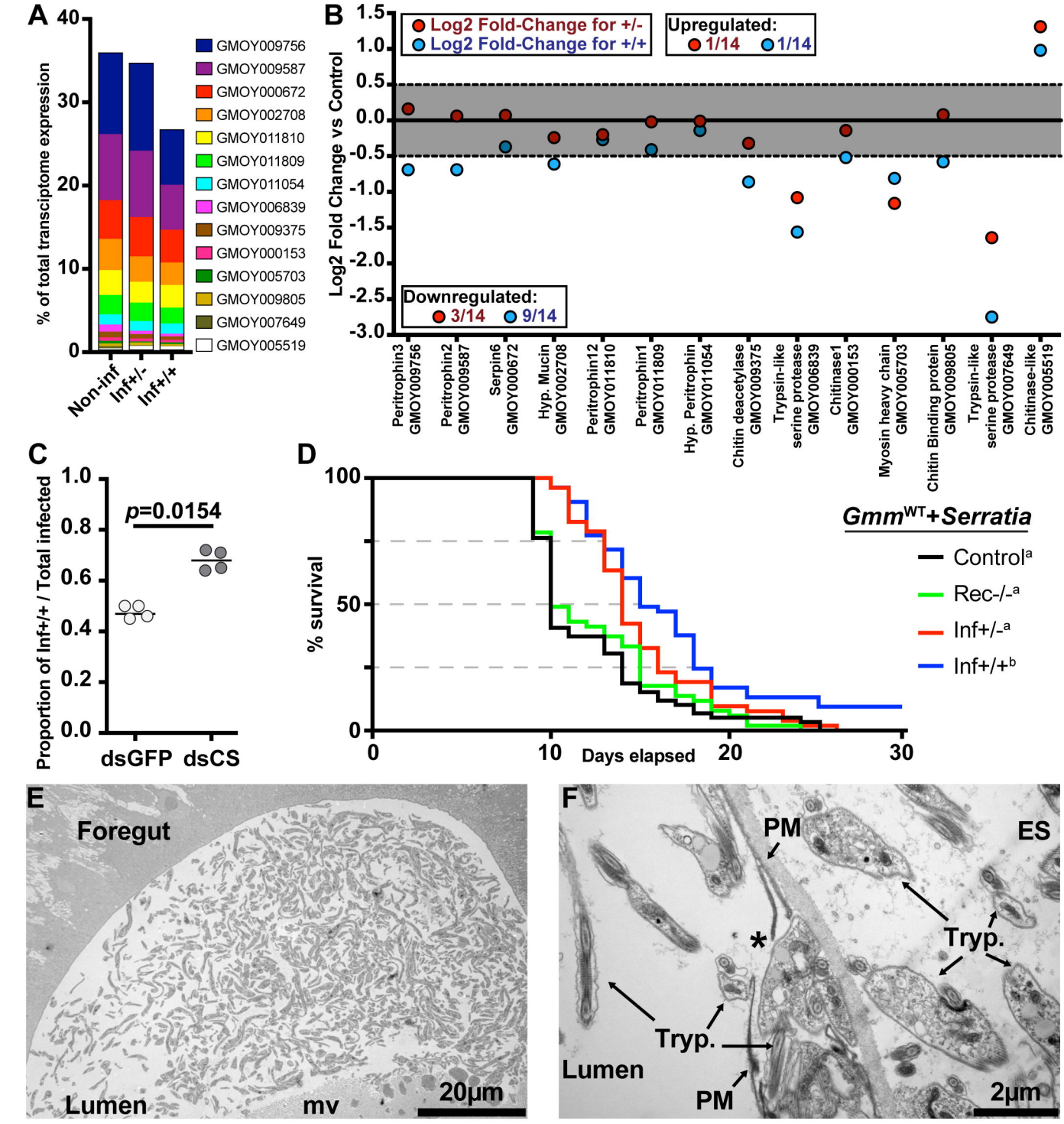
A
% of total transciptome expression
GMOY009756
GMOY009587
GMOY000672
GMOY002708
GMOY011810
GMOY011809
GMOY011054
GMOY006839
GMOY009375
GMOY000153
GMOY005703
GMOY009805
GMOY007649
GMOY005519
Non-inf
Inf+/-
Inf+/+
B
Log2 Fold-Change for +/-
Log2 Fold-Change for +/+
Upregulated:
1/14
1/14
Log2 Fold Change vs Control
Downregulated:
3/14
9/14
Peritrophin3 GMOY009756
Peritrophin2 GMOY009587
Serpin6 GMOY000672
Hyp. Mucin GMOY002708
Peritrophin12 GMOY011810
Peritrophin1 GMOY011809
Hyp. Peritrophin GMOY011054
Chitin deacetylase GMOY009375
Trypsin-like serine protease GMOY006839
Chitinase1 GMOY000153
Myosin heavy chain GMOY005703
Chitin Binding protein GMOY009805
Trypsin-like serine protease GMOY007649
Chitinase-like GMOY005519
C
p=0.0154
Proportion of Inf+/+ / Total infected
dsGFP
dsCS
D
% survival
Days elapsed
GmmWT+Serratia
Controla
Rec-/-a
Inf+/-a
Inf+/+b
E
Foregut
Lumen
mv
20µm
F
PM
ES
Tryp.
Tryp.
Lumen
PM
2µm

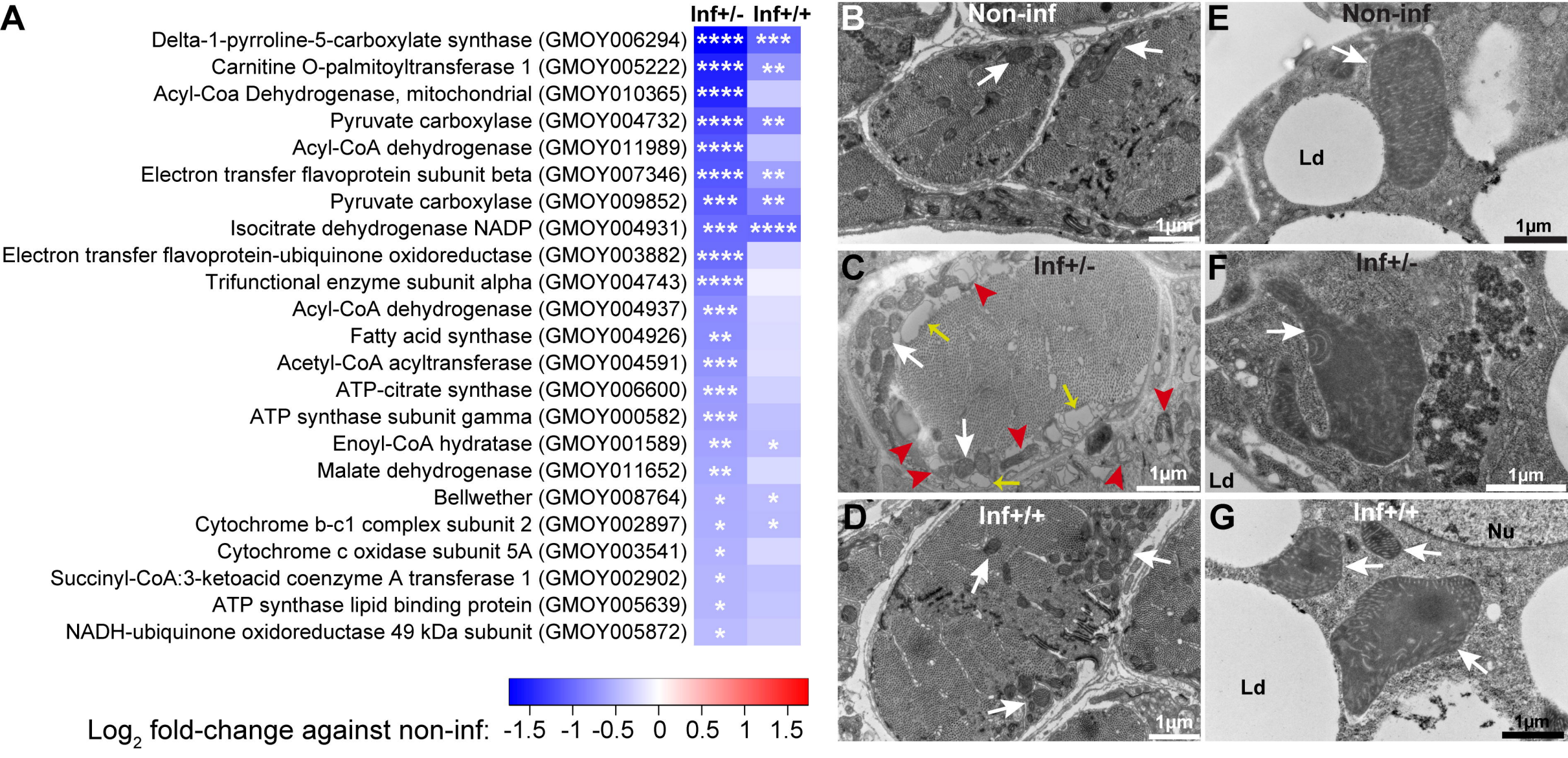
A
Inf+/-
Inf+/+
Delta-1-pyrroline-5-carboxylate synthase (GMOY006294) **** ***
Carnitine O-palmitoyltransferase 1 (GMOY005222) **** **
Acyl-Coa Dehydrogenase, mitochondrial (GMOY010365) ****
Pyruvate carboxylase (GMOY004732) **** **
Acyl-CoA dehydrogenase (GMOY011989) ****
Electron transfer flavoprotein subunit beta (GMOY007346) **** **
Pyruvate carboxylase (GMOY009852) *** **
Isocitrate dehydrogenase NADP (GMOY004931) *** ****
Electron transfer flavoprotein-ubiquinone oxidoreductase (GMOY003882) ****
Trifunctional enzyme subunit alpha (GMOY004743) ****
Acyl-CoA dehydrogenase (GMOY004937) ***
Fatty acid synthase (GMOY004926) **
Acetyl-CoA acyltransferase (GMOY004591) ***
ATP-citrate synthase (GMOY006600) ***
ATP synthase subunit gamma (GMOY000582) ***
Enoyl-CoA hydratase (GMOY001589) ** *
Malate dehydrogenase (GMOY011652) **
Bellwether (GMOY008764) * *
Cytochrome b-c1 complex subunit 2 (GMOY002897) * *
Cytochrome c oxidase subunit 5A (GMOY003541) *
Succinyl-CoA:3-ketoacid coenzyme A transferase 1 (GMOY002902) *
ATP synthase lipid binding protein (GMOY005639) *
NADH-ubiquinone oxidoreductase 49 kDa subunit (GMOY005872) *
Log2 fold-change against non-inf: -1.5 -1 -0.5 0 0.5 1 1.5
B
Non-inf
1µm
E
Non-inf
Ld
1µm
C
Inf+/-
1µm
F
Inf+/-
Ld
1µm
D
Inf+/+
1µm
G
Inf+/+
Nu
Ld
1µm

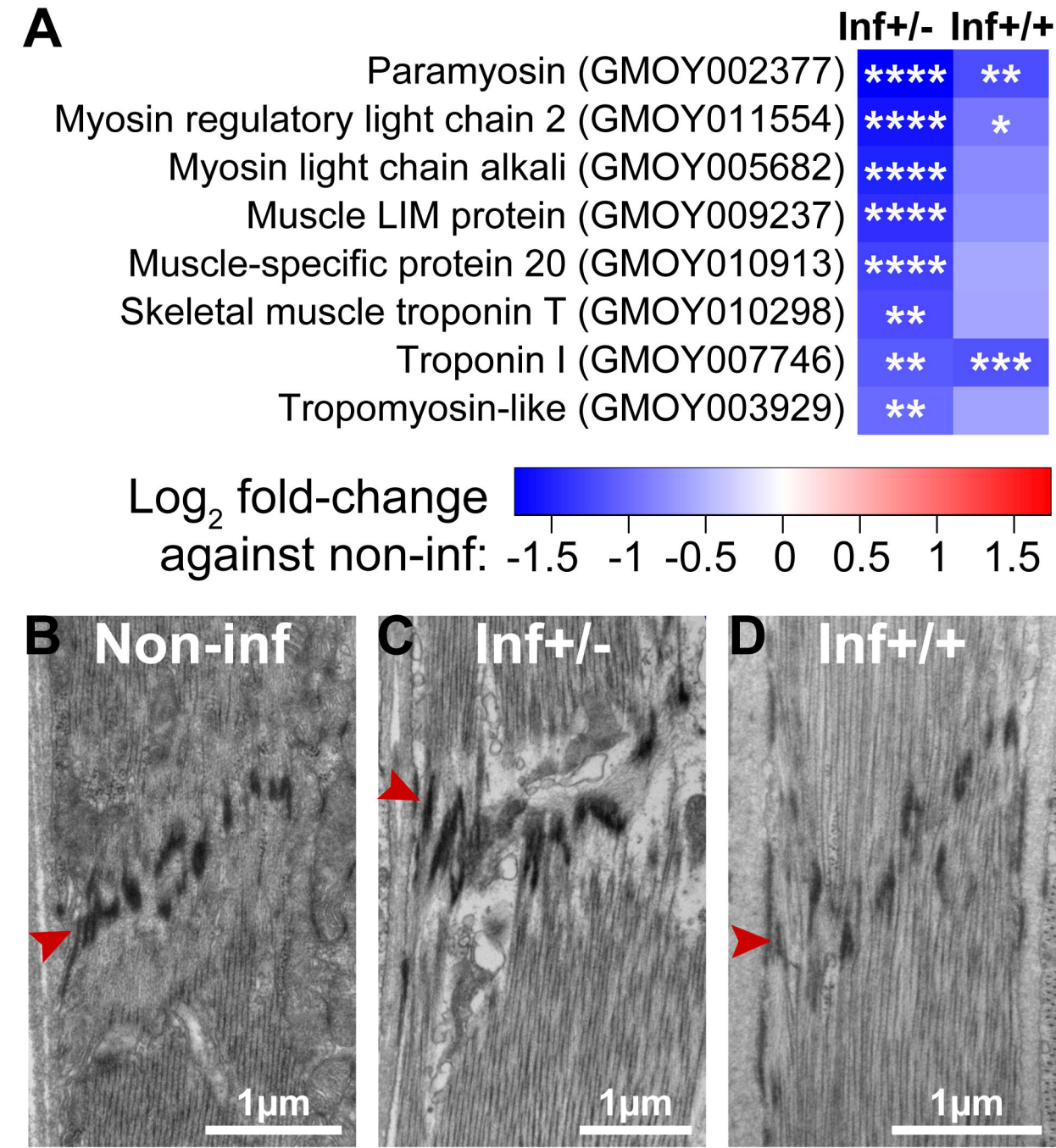
A
Inf+/-
Inf+/+
Paramyosin (GMOY002377)
****
**
Myosin regulatory light chain 2 (GMOY011554)
****
*
Myosin light chain alkali (GMOY005682)
****
Muscle LIM protein (GMOY009237)
****
Muscle-specific protein 20 (GMOY010913)
****
Skeletal muscle troponin T (GMOY010298)
**
Troponin I (GMOY007746)
**
***
Tropomyosin-like (GMOY003929)
**
Log2 fold-change against non-inf:
-1.5 -1 -0.5 0 0.5 1 1.5
B Non-inf
1µm
C Inf+/-
1µm
D Inf+/+
1µm

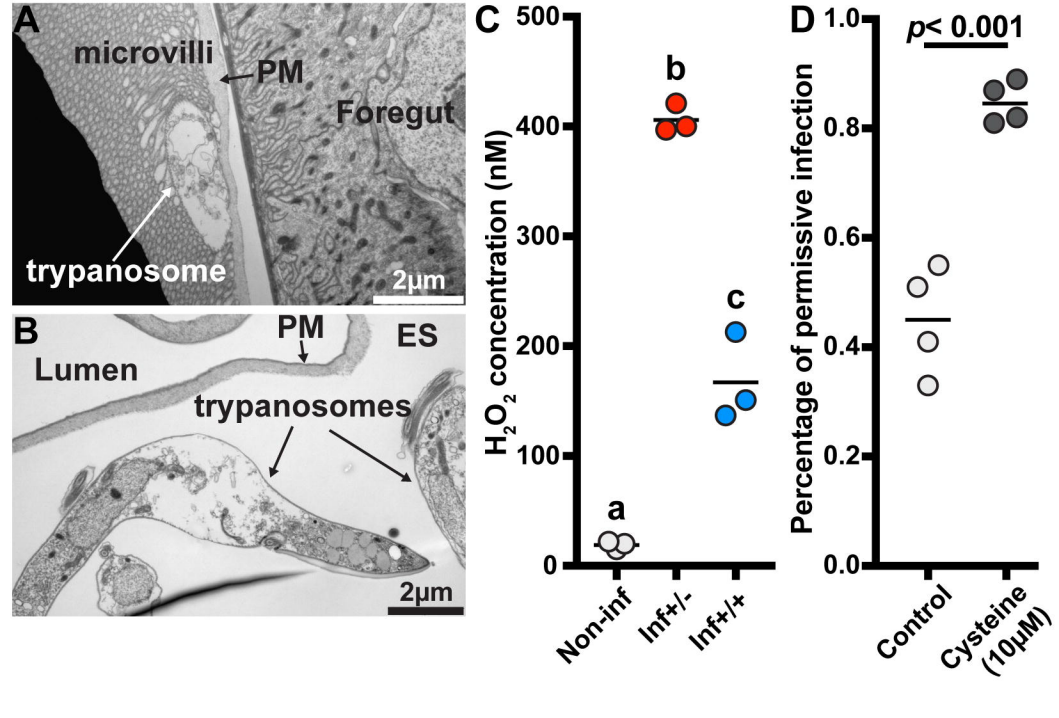
A
microvilli
PM
Foregut
trypanosome
2µm
B
PM
ES
Lumen
trypanosomes
2µm
C
500
400
300
200
100
0
H_2O_2 concentration (nM)
a
b
c
Non-inf
Inf+/-
Inf+/+
D
1.0
0.8
0.6
0.4
0.2
0.0
Percentage of permissive infection
p< 0.001
Control
Cysteine (10µM)

Permissive infection (inf+/+)

Non-Permissive infection (inf+/-)

To Salivary Glands

1

2

3

4

5

6

7

8

Muscles

Cardia midgut epithelium

ES

PM

Lumen

Cardia foregut epithelium

Mitochondrion

Mitochondrial vacuolation and swelling

PM constituents

Sarcoplasmic dilatation

ROI

Live trypanosome

Dead trypanosome

Trypanosome-derived particles